Numerical Simulation of the Load Transfer Mechanism at UHPC-UHPC Interface

Ali A. Semendary, Ph.D. (corresponding author) – Research Associate, University of Manitoba, Department of Civil Engineering, Winnipeg, MB, CA, Email: Ali.Semendary@umanitoba.ca

Dagmar Svecova, Ph.D., P.Eng. – Professor, University of Manitoba, Department of Civil Engineering, Winnipeg, MB, CA, Email: Dagmar.Svecova@umanitoba.ca

Abstract

Ultrahigh performance concrete (UHPC) has been used in a different range of applications, especially in bridge construction, due to its outstanding mechanical properties, ductility, and long-term durability. There has been a rapid increase in the use of precast UHPC systems. The weakest link in the UHPC precast system is the interface between the precast UHPC components. The interfacial bond performance between UHPCs cast at different times plays a key role to ensure a load transfer and to achieve a composite behaviour. It has been experimentally proven that the exposed fibers using pressure washing or grooved surface preparations are an effective method to treat the UHPC–UHPC interface, but the numerical simulation and appropriate modeling remain under-investigated. This study focuses on the numerical simulation of the interfacial bond strength using finite element modeling (FEM). The traction-separation relationship with parameters derived from an experimental program were used to calibrate and validate the FE model. The model used information obtained from specimens tested under tensile, shear, and a combination of compression-shear stresses. This paper discusses the modeling of the interface between UHPC cast at different times to accurately simulate the failure mode and load transfer at the interface.

Keywords: Bond, FE model, Traction-separation, Interface, Adhesion/Cohesion, Load Transfer

1. Introduction

Ultra-high-performance concrete (UHPC) possesses outstanding mechanical properties such as compressive strength over 120 MPa, effective cracking tensile strength over 5 MPa, high ductility due to fiber bridging, low permeability, and superior durability (Graybeal et al. 2020). The localization tensile strain value must be at least 0.0025 to be distinguishable from fiber reinforced concrete (El-Helou et al. 2022). The UHPC sustained tensile strength depends on fiber content, type, and orientation. The UHPC also provides a superior bond with rebar which significantly reduced the required embedment length (Yuan and Graybeal 2014). There has been a rapid increase in the use of precast UHPC systems such as bridge decks, girders, and overlays. Similar to regular concrete, the construction/cold joints are required in most applications due to construction or design requirements. Several experimental studies have proven that the fiber exposure at the interface using pressure washing, chiseling or steel wire mesh methods led to better bond strength under different stress conditions (Jang et al. 2017; Li et al. 2019; Lu et al. 2022; Semendary et al. 2022). Meanwhile, the interface is still the weakest link in the structural system and most of the experimental studies report interfacial failures between precast UHPC components

(Zhao et al. 2022; Xiao et al. 2022). Several studies investigated the bond performance between precast UHPC and cast in place UHPC under different stress conditions. Ding et al. (2022) investigated the bond performance between precast and cast in place UHPCs using as-cast, chiseled (some fiber exposed) and grooved surface preparations. The results indicated that the groove surface preparation that utilized 8 mm× 10 mm groove system provided the highest bond under all stress conditions. Lu et al. (2022) investigated the bond performance of as-cast, chipped and steel wire mesh surface preparations. Both chipping and steel wire mesh provided bond strength that exceed the as cast surface preparation. Semendary et al. (2022) also demonstrated that exposed fibers and groove surface preparations experienced the highest bond strength compared with the other surface preparations. Haber et al. (2022) confirmed that the fiber exposure technique using retarder on the formwork with subsequent power washing of the surface after demolding is more effective method than formwork liner for precast and cast in place UHPC systems. Studies presenting numerical simulation and FE modeling of UHPC-UHPC interface are lacking in current literature. Furthermore, bond-slip relationship that can be used to better model the load transfer at the interface using traction separation under tension and shear stresses are still needed.

2. Validation Study - Details of The Existing Experimental Work

To extract the bond -slip relationship and to represent the bond failure under different stress conditions, experimental testing is needed. Semendary et al. (2022) investigated the bond performance of five different UHPC surface preparations i.e., smooth, sandblasting, needle scaler, pressure washing and grooves. Three different test methods (i.e., direct tension, bi-shear, and slant shear) were used to investigate the bond the interface. The direct tension test was conducted according to the ASTM C1404/C1404M-98) (ASTM 2003) using 75 mm by 150 mm composite cylinder while the bi-shear test was conducted using 150 mm cubic specimens. The slant shear test was conducted using prisms with different slants (i.e., 20°, 25° and 30° with vertical). Commercial UHPC mix with 2% steel fiber was used for both precast and cast in place UHPCs. The UHPC reached a compressive strength of 172.2 MPa and 165.2 MPa at the day of testing for both UHPCs. The fiber exposure using on form retarder and then pressure washing after 24 hours was confirmed to provide outstanding bond. The advantage of the method is that it is widely accepted and easily applicable in the field. The bond versus dilation relationship from the specimens are shown in Figure 1a. The bond dilation relationship was extracted by using the average of the ultimate strength and the dilation of the specimens. The specimens under direct tension failed at the interface. The bond slip relationship shows that after the peak stress that was recorded after the first crack, there was a 50% post-cracking capacity in all the direct tension specimens. This is direct effect of fibers crossing the crack, allowing development of fiber bridging mechanisms as shown in Figure 1a and 2a. The bi-shear specimens load-slip curves included three distinct regions: linear elastic region with no slip until the first crack, nonlinear region with evidence of slippage until interfacial failure and potential increase in the capacity until ultimate failure as shown in Figure 1b. After the interfacial failure, the load transferred to the monolithic part of the specimen which caused an increase in load carrying capacity. Therefore, the bond-slip relationship was based on the load at the point of interfacial failure only and did not include the ultimate load as it was caused by the test set up. The failure modes from bi-shear test are shown in Figure 2b. The slant shear specimens represented the bond strength under combined compression and shear stresses.

Only the specimen that experienced interfacial failure mode was considered in the current study because it reported the bond strength of the interface. The shear stress-slip at the interface in the slant shear specimens is shown in Figure 1c and the failure mode is shown in Figure 2c. More details about the experimental work can be found in Semendary et al. (2022).

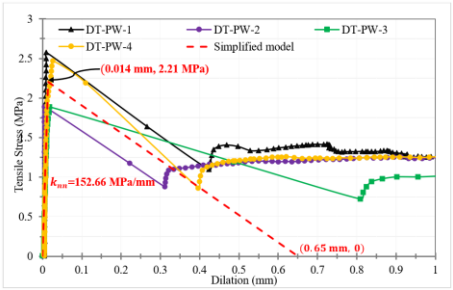

(a)

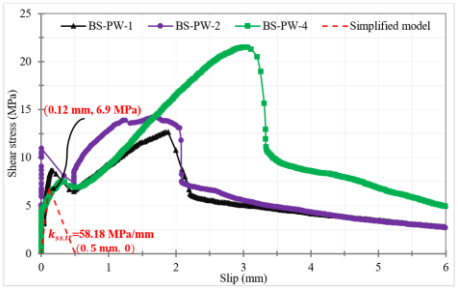

(b)

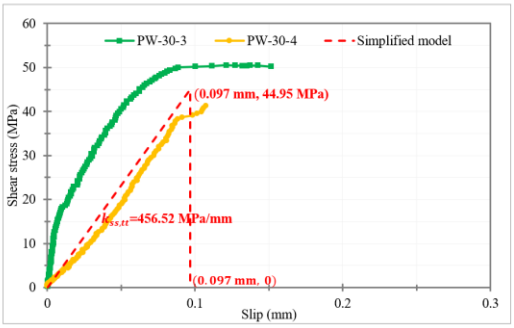

(c)

Figure 1 Shear stress versus dilation/slip: (a) Direct tension; (b) Bi-shear, and (c) Slant shear

(a)

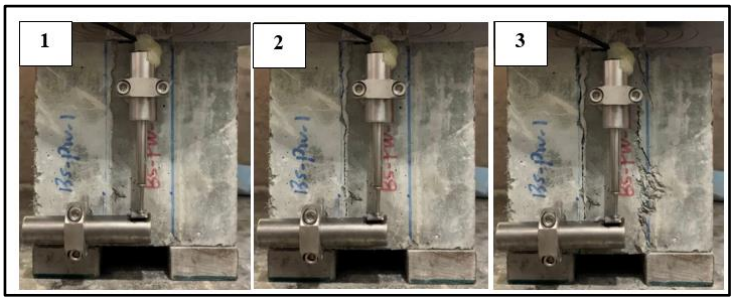

(b)

(c)

Figure 2 Failure mode: (a) Direct tension; (b) Bi shear and (c) Slant shear

3. FE Model

A detailed 3D nonlinear finite element (FE) model was built using a commercial software package to simulate the direct tension, bi-shear, and slant shear tests. The direct tension specimen was modeled using a 76 mm by 152 mm composite specimen with cold joint at the mid height to represent the experimental testing as shown in Figure 3a. For the bi-shear specimens, the 150 mm cube with loaded and supported plates were modeled as shown in Figure 3b. The thickness of the precast UHPC portion of the specimen was 100 mm, while the cast in place UHPC thickness was 50 mm. For the slant shear, prisms with dimensions of 75 mm by 75 mm by 280 mm were used in the experimental program. The slant in these specimens was 30° as shown in Figure 3c. Steel plate was used in the experimental program to support and distribute the load. Deformable solid elements with eight-node linear reduction integrals (C3D8R) were employed for the simulation of UHPC, the loading plates and supports. After a mesh sensitivity analysis, UHPC has been meshed with appropriate mesh size that led to excellent comparison with the experiment. Translation in all directions were prevented in the modeling of the support while the load was applied using displacement control to simulate the applied load during the testing program.

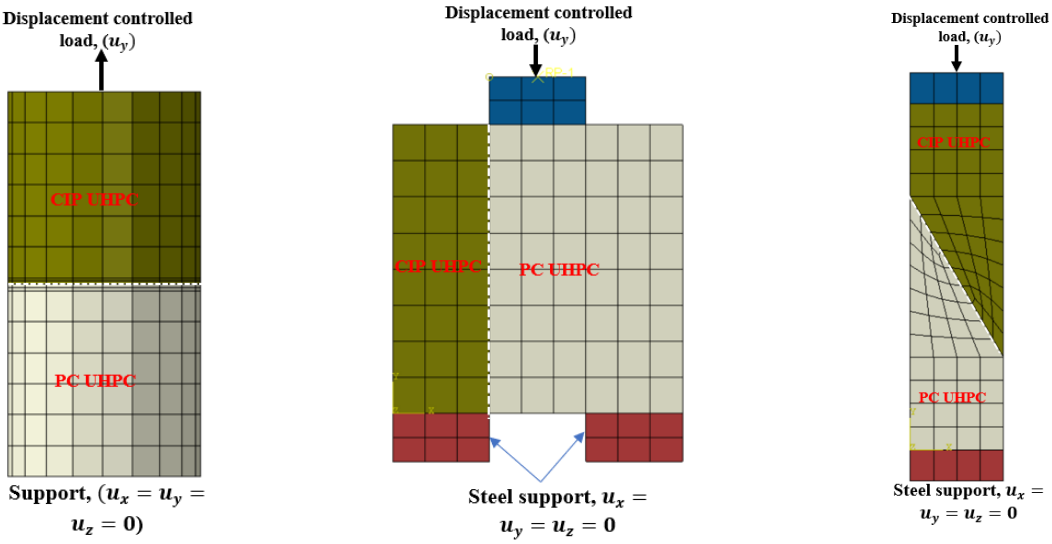

Figure 3 FE model: (a) Direct tension; (b) Bi-shear and (c) Slant shear

3.1. Material constitutive model

The concrete damage plasticity (CDP) model was used to model the UHPC material due to its strong capability in representing the stress failure criteria of the concrete in compressive, tension and damage indices. The modulus of elasticity (E) was calculated using the equation (1) proposed by El-Helou et al. (2022) and it is suitable for the UHPC with compressive strength between 127 and 200 MPa. The authors also suggested a Poisson's ratio of 0.15 as it was found in literature to be varied between 0.1 and 0.2 (El-Helou et al. 2022)

$$E = 900 f_c'^{0.33} \quad (1)$$

For UHPC in compression and to extract the stress-strain model for UHPC in compression, the model proposed by Graybeal (2007) was used. The stress-strain relationship is defined in Equations 2&3, which shows that the stress and strain are related by the modulus of elasticity and a reduction factor α, which defines the decrease in the actual stress from the linear elastic stress.

$$f_c = \begin{cases} \varepsilon_c E & 0 \le f_c \le 0.5 f_c' \\ \varepsilon_c E(1-\alpha) & 0.5 f_c' \le f_c \le f_c' \end{cases} \quad (2)$$

$$\alpha = 0.011 e^{\frac{\varepsilon_c E}{0.44 f_c'}} - 0.011 \quad (3)$$

Where: f_c' , α are compressive strength and reduction factor, respectively.

The UHPC in tension experienced two types of behaviors: elastic-plastic or bilinear stress-strain (hardening) behavior depending on testing method, fiber content, fiber type and fiber orientation. There are several models proposed to model the UHPC in tension. The first model was proposed by Zhang et al. (2015) and it is the most common model used by other researchers. The model consists of two stages of stress strain response and one stage of stress-crack opening relationship. The bilinear stress–strain law is used to describe the elastic behavior and hardening of UHPC and the stress–crack opening law is used to describe the softening behavior. The model was proposed after investigating the effect of the hybrid steel fibers (straight and hooked end) and fiber content (2, 2.5, 3 and 3.5%). The compressive strength was between 146.8 MPa to 176.2 MPa and tensile strength was 6.76 MPa and 7.91 MPa. The study by El-Helou et al. (2022) proclaimed that the UHPC in tension may experience elastic plastic or strain hardening behaviours depending on the fiber type, ratio, and fiber orientation. The following expressions were used to model the tensile behaviour by assuming elastic-plastic stress strain model. The stress curve exhibits linear behaviour until the maximum tensile stress is reached, after which the stress is taken as a constant value of f_{ct} up to the ultimate tensile strain.

$$f_t = \begin{cases} \frac{f_{ct}}{\varepsilon_a}\varepsilon & 0 < \varepsilon \le \varepsilon_{ct} \\ f_{ct} & \varepsilon_{ct} < \varepsilon \le \varepsilon_{pc} \end{cases} \quad (4)$$

Where: f_{ct} is the tensile strength, ε_{ct} elastic tensile strain and ε_{pc} is the limited tensile strain. The steel plate was defined using the modulus of elasticity of 200,000 MPa and Poisson's ratio of 0.3. In order to define the CDP in Abaqus, there are five parameters that need to be defined which includes the dilation angle ψ, flow potential eccentricity ε, the ratio of initial equibiaxial compressive yield stress to initial uniaxial compressive yield stress f_{bo}/f_{co}, the ratio of the second stress invariant on the tensile meridian to that on the compressive meridian κ and viscosity parameter μ. The parameters used in the current study are shown in Table 1 (Feng et al. 2022).

Table 1: Concrete damaged plasticity model (CDP)parameters for nonlinear FE model

Dilation angle	Eccentricity	f_{b0}/f_{c0}	k	Viscosity parameter
30°	0.1	1.16	0.6667	0.005

3.2. Interface

The interface at UHPC-UHPC cold joint can be modeled using different techniques in Abaqus using tie, traction separation or friction models. In the tie model, which assumes a perfect bond at the interface, the interface is assumed to work as monolithic. This assumption is invalid in the current study, because separation was noticed in all tests and under different stress conditions. The second model is using traction separation model by considering the adhesion/ cohesion components in load transfer mechanism. The friction model ignores adhesion and relies on the friction only through the finterlock and is increased by the presence of compressive force acting across the interface. The friction model does not allow any penetration or transfer of tensile stress across the interface. In the current study the second model was selected and validated using the FE model to be used in the future to model the load transfer at UHPC-UHPC interface. The traction separation law consists of three parts: linear elastic behavior, damage initiation and damage evolution. In the absence of any bond failure, the behavior of the contact surface is assumed to be linear elastic and this behavior will terminate with the occurrence of the failure. The linear elastic behavior is described by a constitutive matrix, traction, and separations as shown in Figure 4. The variables t_n; t_s, and t_t represent the peak values of the nominal stress when the deformation is either purely normal to the interface, purely in the first shear direction, or purely in the second shear direction, respectively. The parameters k_{nn}, k_{ss}, and k_{tt}, are the normal and tangential stiffness components that relate to the normal and shear separation across the interface before the initiation of damage. The corresponding separations are identified by δ_n, δ_s, and δ_t. When the quadratic stress-based damage criterion for a cohesive surface is satisfied, damage occurs. The variables t_n^0; t_s^0, and t_t^0 represent the maximum values for contact stresses from Figure 1.

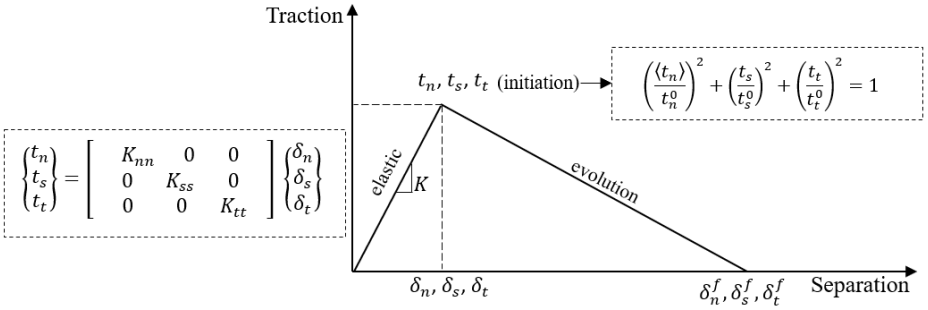

Figure 4 traction–separation response (adopted from Farouk et al 2022)

Once damage initiation has occurred, damage evolution is determined based on the total fracture energy (G_c) or the total plastic displacement at failure (δ_n^f). The damage evolution softening response can be either linear, exponential, or user defined. In the current study the linear damage evolution softening response was used. During the modelling any convergence difficulty issues may be overcome by defining the viscous regularization of the constitutive equations. To define the traction separation parameters, the experimental results from Figure 1 were used for both tensile and bi-shear test. For slant shear test due to the presence of the compressive stress, the friction model was considered in addition to the traction separation model. In the friction model, the normal behavior was defined using "hard" contact in Abaqus while the tangential behavior was defined using the "penalty" option with friction coefficient of 1.43 for exposed fiber surface preparation (Semendary et al. 2022).

4. Results

Three different FE models were run to calibrate the proposed bond slip relationship under different stress status. The FE model results indicate a very good agreement with the average experimental load and dilation/slip at the interface as shown in Table 2. The failure mode for the three test types near the failure is shown in Figure 5. The FE model indicated interfacial failure after meeting the failure criteria of traction separation model. The interface failure occurred when the damage criterion for a cohesive surface is satisfied. For the slant shear stress, the model was run with/without friction and the results indicated that the friction must not be ignored as it appeared to contribute to the load transfer after cohesive failure. The failure mode also shown in Figure 5c.

Table 2 Results of FE model

Test method	Average ultimate load		Exp./FE	Dilation/Slip		Exp./FE
	Experiment (kN)	FEA (kN)		Experimental	FEA	
Direct tension	10.01	9.90	1.01	0.014	0.015	0.93
Bi-Shear	407.0	389.0	1.05	0.155	0.159	0.97
Slant shear	595.7	564.02	1.05	0.097	0.158	0.61

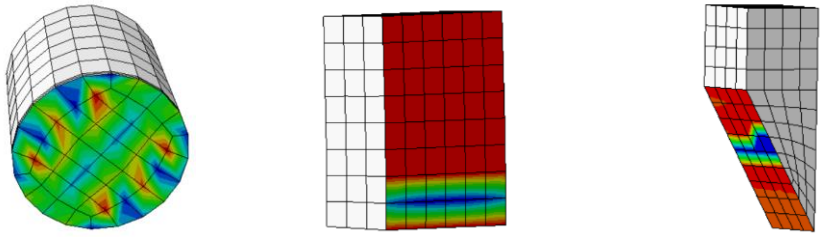

(a) (b) (c)

Figure 5 Damage initiation criteria failure mode: (a) Direct tension; (b) Bi shear and (c) Slant shear

5. Conclusions

A nonlinear FEM for simulating the UHPC-UHPC interface was established and verified based on the test results using the traction separation models. The FE results showed good agreement with experimental results which demonstrated the validity of the proposed model to capture the load transfer and failure at UHPC-UHPC interface. Based on the results, the bond-dilation/slip models under tension, shear and combination of compression and shear are proposed to model UHPC-UHPC interface with exposed fiber surface preparation as shown in Figure 6.

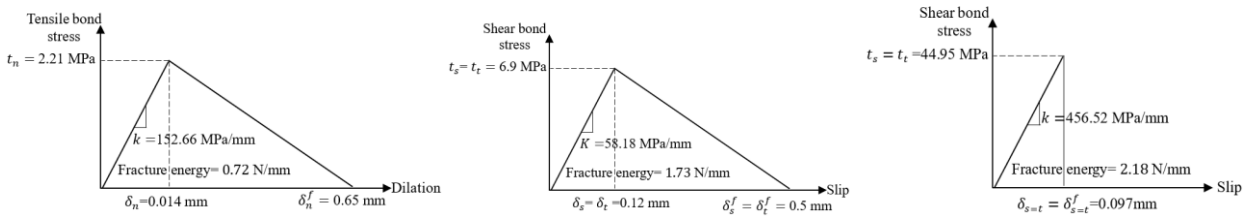

(a) Tension (b) Direct shear (c) Compression-shear

Figure 6 Proposed bond-dilation/slip relationship for exposed fiber surface treatment

6. References

- Ding, J., Zhu, J., & Kang, J. (2022, September). Bonding properties and mechanism of the interface between precast UHPC and post-cast UHPC. In Structures (Vol. 43, pp. 822-833). Elsevier.
- El-Helou, R. G., Haber, Z. B., & Graybeal, B. A. (2022). Mechanical Behavior and Design Properties of Ultra-High-Performance Concrete. ACI Materials Journal, 119(1).
- Graybeal, B., Brühwiler, E., Kim, B. S., Toutlemonde, F., Voo, Y. L., & Zaghi, A. (2020). International perspective on UHPC in bridge engineering. Journal of Bridge Engineering, 25(11), 04020094.
- Haber, Z. B., McDonagh, M., Foden, A., & Sadasivam, S. (2022). Ultra-High Performance Concrete (UHPC) Overlays: An Example of Lifecycle Cost Analysis (No. FHWA-HRT-23-012).
- Jang, H. O., Lee, H. S., Cho, K., & Kim, J. (2017). Experimental study on shear performance of plain construction joints integrated with ultra-high performance concrete (UHPC). Construction and Building Materials, 152, 16-23.
- Li, C., Feng, Z., Ke, L., Pan, R., & Nie, J. (2019). Experimental study on shear performance of cast-in-place ultra-high performance concrete structures. Materials, 12(19), 3254.
- Lu, K., Pang, Z., Xu, Q., Yao, Y., Wang, J., & Miao, C. (2022). Bond strength between substrate and post-cast UHPC with innovative interface treatment. Cement and Concrete Composites, 133, 104691.
- Semendary, A. A., Kriegl, A. J., & Svecova, D. (2022). Experimental study on bond performance at UHPC-UHPC cold joints. Construction and Building Materials, 344, 128237.
- Xiao, J. L., Guo, L. X., Nie, J. G., Li, Y. L., Fan, J. S., & Shu, B. A. (2022). Flexural behavior of wet joints in steel-UHPC composite deck slabs under hogging moment. Engineering Structures, 252, 113636.
- Yuan, J., & Graybeal, B. (2015). Bond of Reinforcement in Ultra-High-Performance Concrete. ACI Structural Journal, 112(6).
- ASTM. (2003). "Standard test method for bond strength of adhesive systems used with concrete as measured by direct tension (withdrawn 2010)." C1404/C1404M-98, West Conshohocken, PA.
- Zhang Z, Shao XD, Li WG et al (2015) Axial tensile behavior test of ultra high performance concrete. China J Highw Transp 8:50
- Feng, Z., Li, C., Ke, L., & Yoo, D. Y. (2022, November). Experimental and numerical investigations on flexural performance of ultra-high-performance concrete (UHPC) beams with wet joints. In *Structures* (Vol. 45, pp. 199-213). Elsevier.
- Graybeal BA. Compressive behavior of ultra-high-performance fiber-reinforced concrete. ACI Mater J 2007;104(2):146–52.
- Farouk, A. I. B., Zhu, J., & Yuhui, G. (2022). Finite element analysis of the shear performance of box-groove interface of ultra-high-performance concrete (UHPC)-normal strength concrete (NSC) composite girder. *Innovative Infrastructure Solutions*, *7*(3), 212.